Featured in Physics

Pressure-Induced Superconductivity In Polycrystalline $La_3Ni_2O_{7-\delta}$

G. Wang,[1,2,*] N. N. Wang,[1,2,*,†] X. L. Shen,[3,*] J. Hou,[1,2] L. Ma,[1,4,5] L. F. Shi,[1,2] Z. A. Ren,[1,2] Y. D. Gu,[1,2] H. M. Ma,[3] P. T. Yang,[1,2] Z. Y. Liu,[1,2] H. Z. Guo,[4,5] J. P. Sun,[1,2] G. M. Zhang,[6] S. Calder,[7] J.-Q. Yan,[8] B. S. Wang,[1,2] Y. Uwatoko,[3] and J.-G. Cheng[1,2,‡]

[1]*Beijing National Laboratory for Condensed Matter Physics and Institute of Physics, Chinese Academy of Sciences, Beijing 100190, China*
[2]*School of Physical Sciences, University of Chinese Academy of Sciences, Beijing 100190, China*
[3]*Institute for Solid State Physics, University of Tokyo, Kashiwa, Chiba 277-8581, Japan*
[4]*Key Laboratory of Materials Physics, Ministry of Education, School of Physics and Microelectronics, Zhengzhou University, Zhengzhou 450052, China*
[5]*Institute of Quantum Materials and Physics, Henan Academy of Sciences, Zhengzhou 450046, China*
[6]*State Key Laboratory for Low dimensional Quantum Physics, Department of Physics, Tsinghua University, Beijing 100084, China*
[7]*Neutron Scattering Division, Oak Ridge National Laboratory, Oak Ridge, Tennessee 37831, USA*
[8]*Materials Science and Technology Division, Oak Ridge National Laboratory, Oak Ridge, Tennessee 37831, USA*

(Received 19 October 2023; revised 18 December 2023; accepted 22 January 2024; published 7 March 2024)

We synthesized polycrystalline $La_3Ni_2O_{7-\delta}$ ($\delta \approx 0.07$) samples by using the sol-gel method without postannealing under high oxygen pressure, and then measured temperature-dependent resistivity under various hydrostatic pressures up to 18 GPa by using the cubic anvil and two-stage multianvil apparatus. We find that the density-wave-like anomaly in resistivity is progressively suppressed with increasing pressure and the resistivity drop corresponding to the onset of superconductivity emerges at pressure as low as ~6 GPa. Zero resistivity is achieved at 9 GPa below $T_c^{zero} \approx 6.6$ K, which increases quickly with pressure to 41 K at 18 GPa. However, the diamagnetic response was not detected in the ac magnetic susceptibility measurements up to 15 GPa, indicating a filamentary nature of the observed superconductivity in the studied pressure range. The constructed T-P phase diagram reveals an intimate relationship between superconductivity, density-wave-like order, and the strange-metal-like behaviors. The observation of zero-resistance state in the polycrystalline $La_3Ni_2O_{7-\delta}$ samples under high pressures not only corroborates the recent report of superconductivity in the pressurized $La_3Ni_2O_7$ crystals but also facilitates further studies on this emerging family of nickelate high-T_c superconductors.

DOI: 10.1103/PhysRevX.14.011040 Subject Areas: Condensed Matter Physics

I. INTRODUCTION

High-T_c superconductors have been at the forefront of scientific exploration due to their immense potential for transformative technological applications. The groundbreaking discovery of cuprate high-T_c superconductors [1,2], where superconductivity emerges through doping Mott insulators with strong electron correlations [3,4], has motivated numerous endeavors in the past decades to unveil its mechanism and to find more superconducting (SC) families with high T_c. Through sharing striking structural and electronic similarities with cuprates, the nickelates with $Ni^+(3d^9)$ electron configuration offer a tantalizing avenue for uncovering new high-T_c superconductors [5–8]. However, superconductivity was not experimentally realized in nickelates until 2019, when the infinite-layer $Nd_{1-x}Sr_xNiO_2$ thin films were found to show superconductivity with T_c around 9–15 K [5]. Since then, considerable dedication has been directed toward finding more nickelate superconductors with higher T_c [9,10]. It was shown that the T_c of $Pr_{0.82}Sr_{0.18}NiO_2$ thin films can be enhanced to over 30 K at 12.1 GPa [11]. However, the superconductivity observed in the nickelate thin films ceases to appear in the bulk samples [12].

Very recently, Sun *et al.* reported the signature of high-temperature superconductivity in $La_3Ni_2O_7$ crystals with T_c up to 80 K at pressures above 14 GPa [13]. In contrast to

*These authors contribute equally to this work.
†Corresponding author: nnwang@iphy.ac.cn
‡Corresponding author: jgcheng@iphy.ac.cn

Published by the American Physical Society under the terms of the Creative Commons Attribution 4.0 International license. Further distribution of this work must maintain attribution to the author(s) and the published article's title, journal citation, and DOI.

the infinite-layer $Nd_{1-x}Sr_xNiO_2$, $La_3Ni_2O_7$ exhibits an exceptionally unique electronic configuration with the nominal oxidation state of $Ni^{2.5+}$, which can be considered as a mixed valence state of $Ni^{2+}(3d^8)$ and $Ni^{3+}(3d^7)$. According to the structural study under high pressure, a structural phase transition from the orthorhombic *Amam* to *Fmmm* space group occurs at about 10–15 GPa, where the interlayer Ni—O—Ni bond angle changes from 168° to 180° [13]. Subsequent high-pressure studies on $La_3Ni_2O_7$ crystals confirmed the presence of a zero-resistance state under better hydrostatic pressure conditions, yet also revealed some issues related to sample-dependent behaviors that remain unclear so far [14,15]. Such a remarkably high T_c has immediately ignited widespread theoretical investigations on the mechanism of high-temperature superconductivity [16–22]. The significance of interlayer exchange between the d_{z^2} orbitals and intralayer hybridization of the d_{z^2} and $d_{x^2-y^2}$ orbitals on the nearest neighbor sites has received substantial attention [23]. In contrast to the extensive theoretical investigations, experimental progress appears to have lagged behind, presumably due to the challenges associated with obtaining high-quality $La_3Ni_2O_7$ single crystals with controlled and homogeneous stoichiometry. Depending on the postannealing process, the oxygen content of $La_3Ni_2O_7$ can vary from $O_{6.35}$ to $O_{7.05}$ [24–29]. In addition, other competitive Ruddlesden-Popper phases are easily formed in the crystals grown using the optical image floating-zone furnace under moderate oxygen pressures [30,31]. It thus becomes an important issue to perform a comprehensive study on the samples with well-controlled quality. Additionally, an open question remains concerning whether superconductivity can be achieved in $La_3Ni_2O_7$ polycrystalline samples subjected to high pressure. Therefore, we are motivated to prepare phase-pure polycrystalline $La_3Ni_2O_{7-\delta}$ samples in which oxygen content and chemical homogeneity can be easily controlled, and then to study the pressure effects on its electrical transport properties under high pressure.

In this work, we synthesized high-quality $La_3Ni_2O_{7-\delta}$ polycrystalline samples with the sol-gel method and then performed a comprehensive study on the transport properties under various hydrostatic pressures up to 18 GPa. We observed superconductivity in the pressurized $La_3Ni_2O_{6.93}$ polycrystalline samples, which exhibit zero resistance in a relatively wide pressure range 9–18 GPa with the superconducting transition temperatures T_c^{zero} up to 41 K and T_c^{onset} up to 78.1 K at 18 GPa. Our results show that high-temperature superconductivity can be achieved in the $La_3Ni_2O_{6.93}$ polycrystalline samples under relatively lower pressures. In addition, the constructed *T-P* phase diagram reveals a close relationship between superconductivity, density-wave-like order, and the strange-metal-like behavior.

II. EXPERIMENT

Polycrystalline $La_3Ni_2O_{7-\delta}$ samples were synthesized by using the sol-gel method and postsintering treatment. A stoichiometric amount of La_2O_3 (Alfa Aesar, 99.99%) and $Ni(NO_3)_2 \cdot 6H_2O$ (Alfa Aesar, 99.99%) were dissolved in nitric acid. After adding some citric acid, the mixture was continuously stirred in a 90 °C water bath for approximately 4 h, resulting in the formation of a vibrant green nitrate gel. This gel was then subjected to overnight heat treatment at 150 °C–200 °C, leading to the formation of a fluffy yellow product. Afterward, the product underwent a presintering step at 800 °C for 6 h to eliminate excess organic components. Subsequently, the resulting powder, with a blackish-gray appearance, was ground and pressed into pellets. These pellets were further sintered in an air environment at temperatures ranging from 1100 °C to 1150 °C for a duration of 24 h, yielding phase-pure polycrystalline $La_3Ni_2O_{7-\delta}$ samples.

The powder x-ray diffraction (XRD) data were collected at room temperature by PANalytical X'Pert PRO with a rotating anode (Cu K_α, $\lambda = 1.5406$ Å). The structural parameters were extracted via refining the XRD pattern with the Rietveld method using the FULLPROF program. Thermogravimetric analysis (TGA) measurement was accomplished in NETZSCH STA 449F3, using a 10% H_2/Ar gas flow of 50 mL/ min with a 7.5 °C/ min rate up to 750 °C. The chemical composition and microstructure analysis were performed on a Hitachi model S-4800 field emission scanning electron microscope (SEM) with an energy-dispersive spectrometer (EDS). Temperature-dependent resistivity $\rho(T)$ at ambient pressure was measured using a Quantum Design Physical Properties Measurement System (QD-PPMS) from 2 to 300 K.

Neutron powder diffraction (NPD) measurements were performed on the HB-2A diffractometer at the High Flux Isotope Reactor (HFIR), Oak Ridge National Laboratory (ORNL) [32,33]. Powder samples of $La_3Ni_2O_{7-\delta}$ were contained within a 6-mm-diameter vanadium sample can and loaded into a closed cycle refrigerator. Data were collected at 295 and 5 K with constant wavelength ($\lambda = 1.54$ Å) measurements performed from the Ge (115) monochromator reflection. The NPD pattern was collected by scanning a 120° bank of 44 ^{3}He detectors in 0.05° steps to give 2θ coverage from 5° to 150°. Rietveld refinements were performed with the FULLPROF program.

We employed the piston-cylinder cell (PCC), cubic anvil cell (CAC), and two-stage 6/8 multianvil (MA) apparatus to measure $\rho(T)$ of $La_3Ni_2O_{7-\delta}$ polycrystalline samples under various hydrostatic pressures up to 18 GPa. The resistivity was measured with the standard four-probe method. Daphne 7373, glycerol, and Fluorinert FC70: FC77 (1:1) were employed as the liquid pressure transmitting medium (PTM) in PCC, CAC, and MA, respectively. The pressure values inside the PCC were estimated by measuring the T_c of Sn according to the equation $P\,(\mathrm{GPa}) = (T_0 - T_c)/0.482$, where $T_0 = 3.72$ K is the T_c of Sn at ambient pressure. The pressure values inside the CAC and MA were estimated from the pressure-loading force calibration curve determined by measuring the structure phase transitions of Bi, Sn, Pb, ZnS, and GaAs at room temperature. As shown in our previous work, the multianvil compression geometry together with the adoption of liquid PTM ensures excellent hydrostatic pressure conditions up to 15 GPa in CAC [34] and ∼20 GPa in MA [35]. The ac susceptibility of $La_3Ni_2O_{7-\delta}$ under various hydrostatic pressures up to 15 GPa was measured with the mutual induction method in the CAC apparatus, where $La_3Ni_2O_{7-\delta}$ polycrystalline samples together with a piece of Pb with a volume ratio of approximately 1∶1 were placed in the same coil. An excitation current of ∼1 mA with a frequency of 317 Hz was applied to the primary coil, and the output signal was picked up with a Standford Research SR830 lock-in amplifier.

III. RESULTS AND DISCUSSION

Figure 1 shows the XRD pattern of the synthesized $La_3Ni_2O_{7-\delta}$ samples. The Rietveld refinement confirms that we obtained a single-phase sample with an orthorhombic structure (space group *Amam*, no. 63). As illustrated in Fig. 1(a), the refinements converged well with reliable factors $R_p = 2.76\%$, $R_{expt} = 2.58\%$, and $\chi^2 = 1.92$. The obtained lattice parameters shown in Fig. 1(a) are in good agreement with those reported previously [13,24,28,29,36]. To determine the oxygen stoichiometry of this compound, we performed TGA measurement in a 10% H_2/Ar flow. As shown in Fig. 1(b), the reduction of $La_3Ni_2O_{7-\delta}$ occurs in two steps with a final formation of a mixture of La_2O_3 and Ni (confirmed by powder XRD). The oxygen stoichiometry of this phase was determined as $La_3Ni_2O_{6.93(1)}$ by calculating the weight loss between the initial and final products.

We performed NPD to further probe the crystalline structure and oxygen content of $La_3Ni_2O_{7-\delta}$. Rietveld refinements are shown in Fig. 1(c). Because of the higher sensitivity to oxygen with neutron scattering, compared to x-ray scattering, the refinements are able to distinguish between the reported space group *Amam* and the higher symmetry *Fmmm* (no. 69) also associated with $La_3Ni_2O_{7-\delta}$. Despite apparently similar refinements to the data, there are reflections only allowed in the *Amam* symmetry. For example, the Bragg peak at $2\theta = 51.8°$ is captured only by the *Amam* space group, as shown in Figs. S1(a) and S1(b) in Supplemental Material [37]. The NPD data also reveal asymmetric Warren-like peak shapes that are typically associated with short-range order. The $(h, k, 0)$ reflections are resolution limited and instead the asymmetric peaks

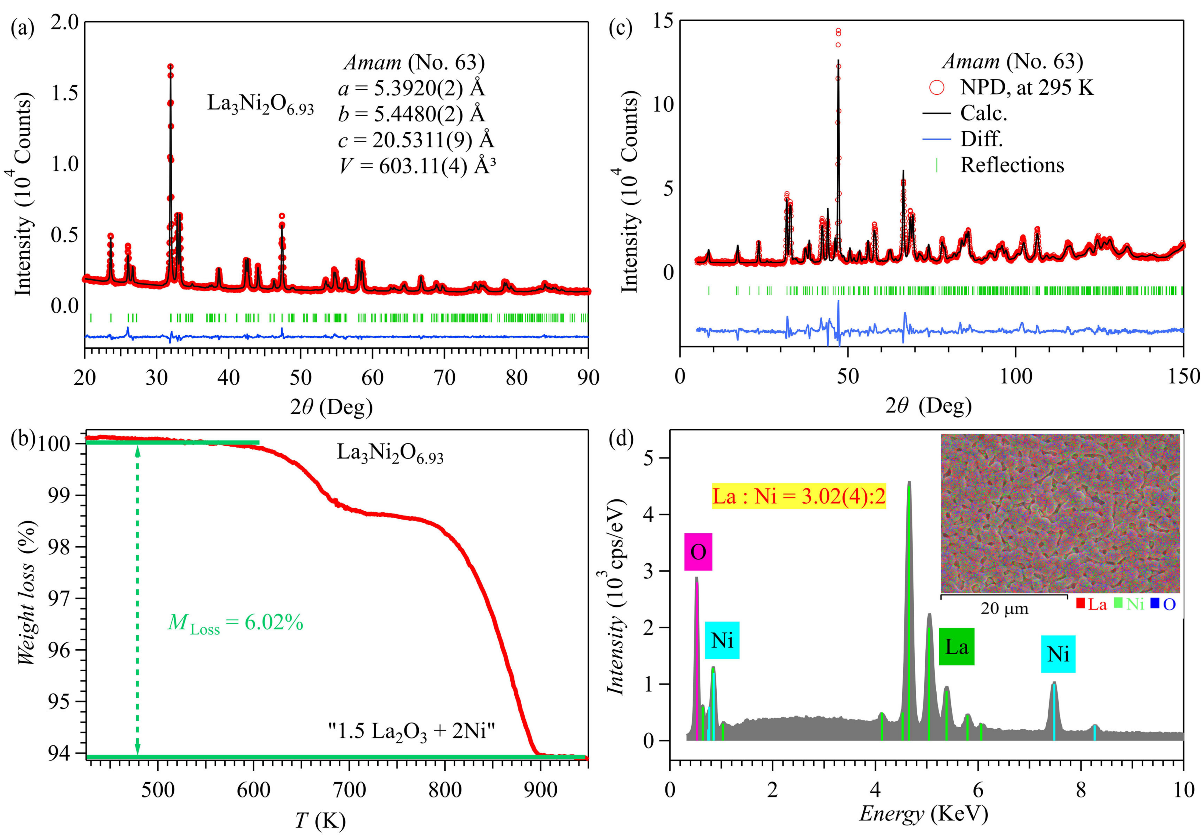

FIG. 1. (a) Rietveld refinements on the room temperature XRD pattern of $La_3Ni_2O_{7-\delta}$ polycrystalline sample. The obtained lattice parameters are shown. The bottom marks and line correspond to the calculated Bragg diffraction positions and the difference between observed and calculated data, respectively. (b) Thermogravimetric curves for $La_3Ni_2O_{7-\delta}$ in 10% H_2/Ar. (c) Rietveld refinements on the NPD pattern of $La_3Ni_2O_{7-\delta}$ polycrystalline sample. (d) The SEM EDS elemental mapping of $La_3Ni_2O_{7-\delta}$ polycrystalline sample.

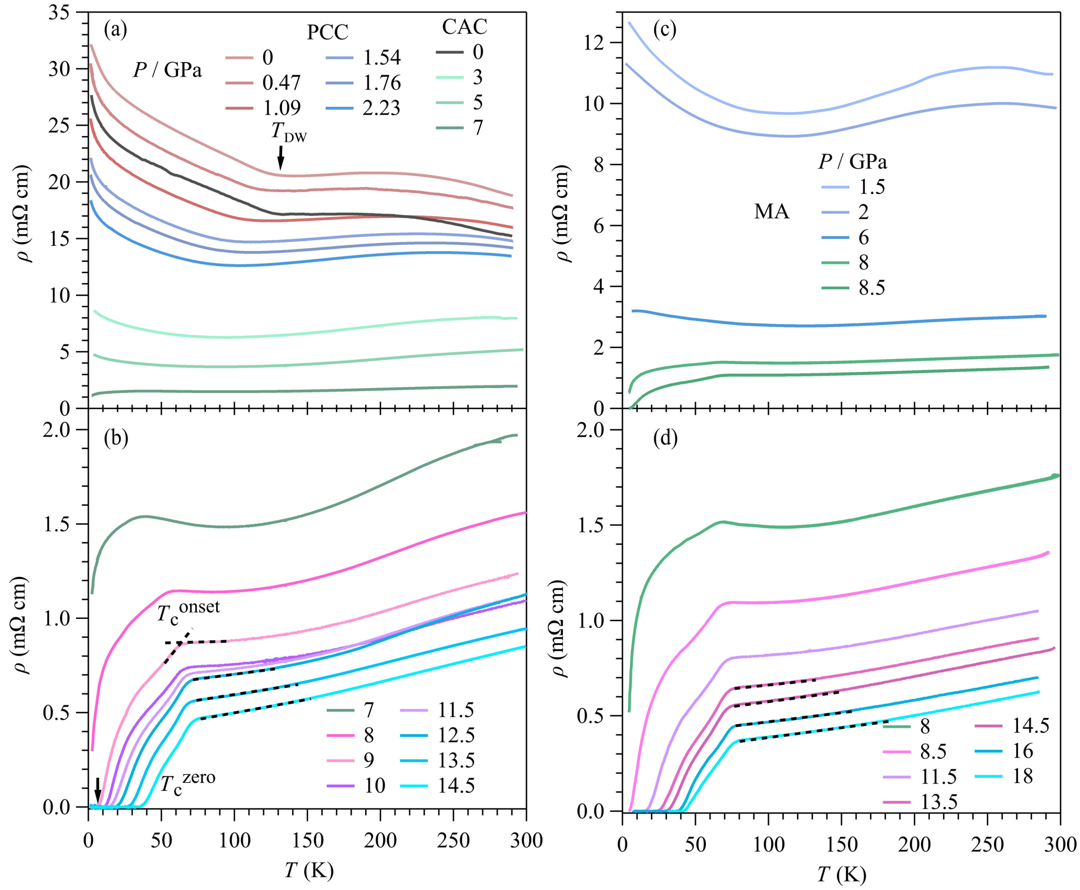

FIG. 2. (a),(b) Temperature dependence of resistivity $\rho(T)$ of $La_3Ni_2O_{6.93}$ polycrystalline sample no. 1 and no. 2 under various hydrostatic pressures up to 14.5 GPa measured in PCC and CAC at the Institute of Physics (IOP) CAS. Here, the T_c^{onset} is determined as the interception between two straight lines below and above the superconducting transitions. (c),(d) Temperature dependence of resistivity $\rho(T)$ of $La_3Ni_2O_{6.93}$ polycrystalline sample no. 3 under various hydrostatic pressures up to 18 GPa measured in MA at the Institute for Solid State Physics (ISSP), University of Tokyo.

appear to be associated with the c axis, which could indicate stacking faults introduced by the oxygen vacancies. The peaks in the 2θ region from 40º to 50º show this behavior, as seen in the inset of Fig. S1(a) [37]. The atypical peak shape limits the fine details that can be extracted on the atomic positions and oxygen content from the Rietveld refinement. Nevertheless, the best fit to the neutron data (Table S1 in Supplemental Material [37]) indicates an oxygen deficient stoichiometry of $La_3Ni_2O_{6.87(5)}$, which is consistent with the TGA measurements of $La_3Ni_2O_{6.93(1)}$. The oxygen vacancies are constrained to the O1 4c Wyckoff position, in line with previous structural studies [36]. Comparison of the NPD patterns at 5 and 295 K reveals no additional scattering associated with any magnetic order or structural transition. Our EDS analysis confirms the chemical composition is $La:Ni = 3.02(4):2$ when setting Ni as 2, which is very close to the expected stoichiometry, and the EDS elemental mapping verifies the uniform distribution of these elements, as seen in Fig. 1(d).

Figure 2(a) shows the $\rho(T)$ of $La_3Ni_2O_{6.93}$ polycrystalline sample no. 1 under various pressures up to 2.23 GPa by using the PCC. At ambient pressure (AP), the $\rho(T)$ exhibits weaker temperature dependence at high temperatures with a broad hump around 220 K, and then displays a metal-insulator-like transition behavior at $T_{DW} \approx 140$ K. The observed “weak insulating” $\rho(T)$ of the $La_3Ni_2O_{6.93}$ polycrystalline sample is similar to the previously reported results, and the metal-insulator-like transition has been attributed to a density-wave (DW) transition [24–27]. As shown in Fig. 2(a), the evolution of the DW transition with pressure can be tracked from the resistivity anomaly. As the pressure gradually increases, the anomaly in $\rho(T)$ and the corresponding T_{DW} determined from the minimum of $\rho(T)$ around the transition continuously moves to lower temperatures, reaching about 103 K at 2.23 GPa. In addition, the DW-like characteristic undergoes broadening as pressure increases, suggesting that the long-range-ordered DW state is partially disrupted by the applied pressure.

To further track the evolution with pressure of the DW transition and to check whether superconductivity can be induced in the $La_3Ni_2O_{7-\delta}$ polycrystalline samples, we perform the resistivity measurements at higher pressures by

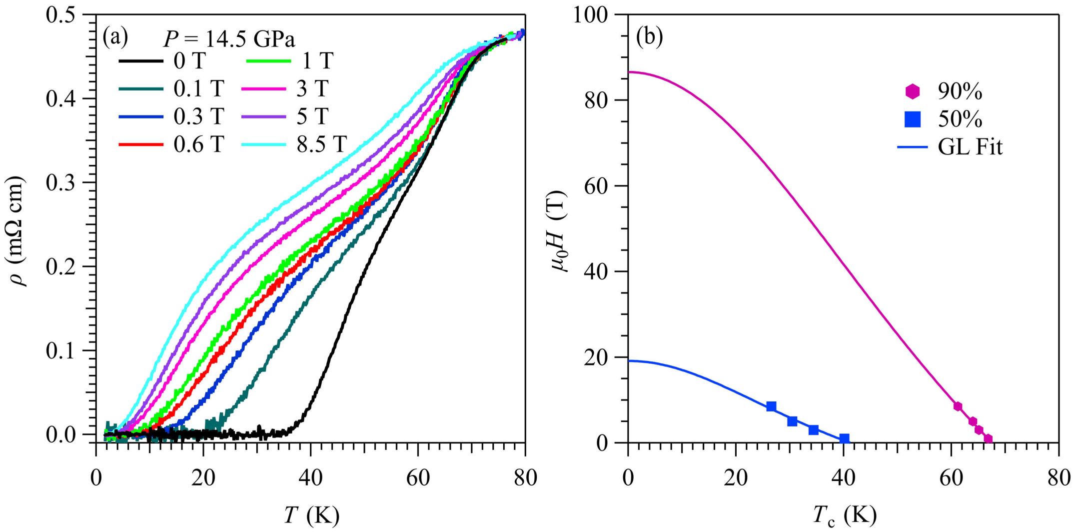

FIG. 3. (a) The low-temperature resistivity $\rho(T)$ at 14.5 GPa of $La_3Ni_2O_{6.93}$ polycrystalline sample no. 2 under various magnetic fields up to 8.5 T. (b) Temperature dependence of the upper critical field $\mu_0 H_{c2}(T)$ for $La_3Ni_2O_{6.93}$ polycrystalline sample at 14.5 GPa. The solid line is the fitting curve by using the formula $H_{c2} = H_{c2}(0)(1-t^2)/(1+t^2)$, where $t = T/T_c$.

employing CAC. Figures 2(a) and 2(b) display the obtained $\rho(T)$ data of sample no. 2 which is prepared in the same batch with sample no. 1, under various pressures up to 14.5 GPa in CAC. At AP, the $\rho(T)$ data exhibit the same behavior as observed in sample no. 1, confirming that our $La_3Ni_2O_{6.93}$ samples are uniform, as verified also by the EDS elemental mapping. As shown in Fig. 2(a), with increasing pressure to about 3 GPa in CAC, the DW transition temperature reaches about 90 K. As the pressure continues to increase, it becomes hard to define due to the broadening of the anomalous feature in resistivity. Interestingly, a distinct behavior characterized by a resistivity drop below 33.8 K emerges at 7 GPa, and this behavior becomes more pronounced shifting to 54.2 K as the pressure is increased to 8 GPa. It is worth noting that this behavior can be sensitively suppressed by external magnetic fields. This feature motivated us to measure $\rho(T)$ in a finer pressure interval from 9 to 14.5 GPa. When the pressure approaches 9 GPa, the shallow minimum feature in $\rho(T)$ fades away and zero resistance is observed at $T_c^{zero} = 6.6$ K, signaling the occurrence of SC transition. This critical transformation between different electronic orders suggests that the DW order and superconductivity compete with each other. Upon further compression, the onset of the superconducting transition T_c^{onset} increases slowly from 63.3 K at 9 GPa to 72.2 K at 14.5 GPa while the zero-resistance temperature T_c^{zero} increases rapidly from 6.6 K at 9 GPa to 35.6 K at 14.5 GPa. Considering that the short-range DW order may partially exist, it can exhibit an inhibitory effect on superconductivity and thus result in a broad SC transition. The observed different pressure dependences of T_c^{onset} and T_c^{zero} may be associate with the competitive relationship between superconductivity and DW. Furthermore, with the enhancement of superconductivity above 9 GPa, the $\rho(T)$ in the normal state exhibits a linear-temperature-dependence behavior, which extends to a wider temperature range as pressure increases, as shown by the dashed lines in Fig. 2(b). Here, T_{sm} was defined as the critical temperature above which the $\rho(T)$ deviates from linearity. This observation is consistent with the previous report on the $La_3Ni_2O_7$ crystals [13,14], signaling a close relationship between strange-metal-like behavior and high-temperature superconductivity in $La_3Ni_2O_{6.93}$ polycrystalline samples.

In order to confirm the reproducibility of the above results and to track the evolution of T_c to higher pressure, we conducted the resistivity measurements of sample no. 3 under various pressures up to 18 GPa by employing the two-stage MA apparatus. As can be seen from Figs. 2(c) and 2(d), the obtained $\rho(T)$ data of sample no. 3 perfectly reproduce the results of samples no. 1 and no. 2. In addition, the $\rho(T)$ data of sample no. 3 measured at 6 GPa show the onset of superconducting transition below 9.7 K. Moreover, the superconducting transition temperatures T_c^{zero} and T_c^{onset} at pressures above 14.5 GPa were observed to continually increase with increasing pressure, reaching 41 and 78.1 K respectively at 18 GPa.

To further determine that the observed resistance drop is truly associated with a superconducting transition, we performed detailed $\rho(T)$ measurements for sample no. 2 at 14.5 GPa under various magnetic fields. As displayed in Fig. 3(a), the superconducting transition of $La_3Ni_2O_{6.93}$ is gradually suppressed to lower temperatures and the transition width becomes broader with increasing magnetic field. Here we define $T_c^{90\%}$ and $T_c^{50\%}$ at each field according to the criteria of 90% and 50% of the corresponding normal-state resistance at T_c^{onset} and plot the temperature dependence of $\mu_0 H_{c2}(T_c)$ in Fig. 3(b). By using the empirical Ginzburg-Landau (GL) equation, the zero-temperature-limit upper critical fields

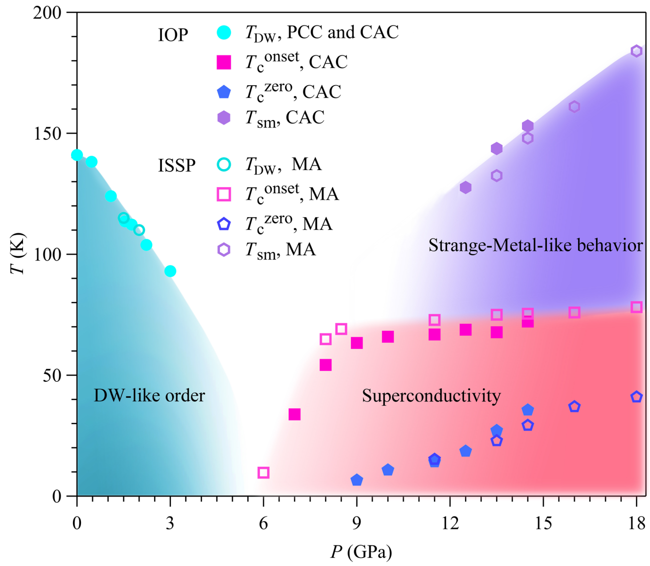

FIG. 4. The T-P phase diagram of the $La_3Ni_2O_{6.93}$ polycrystalline sample. The solid and open circles represent the DW-like transition T_{DW} measured at various pressures using PCC, CAC, and MA. The solid and open squares and pentagons represent the onset and zero-resistance superconducting transition temperatures determined from the present measurements in CAC and MA. The solid and open hexagons represent the critical temperature T_{sm} for the strange-metal-like behavior, above which the $\rho(T)$ curve deviates from linearity.

were determined as $\mu_0 H_{c2}(0) = 86.6$ and 19.1 T for $T_c^{90\%}$ and $T_c^{50\%}$, respectively.

Based on the above high-pressure measurements, we construct the temperature-pressure (T-P) phase diagram of $La_3Ni_2O_{6.93}$ polycrystalline samples, as shown in Fig. 4. In the low-pressure region, the $La_3Ni_2O_{6.93}$ samples exhibit weak insulating behavior below the DW-like transition. As the pressure increases, the DW transition is gradually suppressed from $T_{DW} \approx 140$ K at AP to $T_{DW} \approx 90$ K at 3 GPa, above which the DW-like feature fades away and is replaced by a broad minimum centered around 90 K in resistivity. Such a shallow-valley feature vanishes completely at 9 GPa and the zero-resistance state is realized concomitantly. Upon further increasing pressure, the superconducting transition temperature T_c^{zero} increases rapidly from 6.6 K at 9 GPa to 41 K at 18 GPa and the onset of the superconducting transition T_c^{onset} reaches 78.1 K at 18 GPa. In addition, concomitant with the enhancement of superconductivity in this pressure range, the strange-metal-like behavior seems to be strengthened in the normal state. Our results thus reveal an intimated relationship between superconductivity, DW order, and the strange-metal-like behaviors.

The present work confirmed that high-temperature superconductivity can indeed be achieved in the pressurized $La_3Ni_2O_{6.93}$ polycrystalline samples, and the evolution of superconductivity as a function of pressure shares the same trend as that observed in the $La_3Ni_2O_7$ crystals [13–15] even though the critical pressure for the emergence of superconductivity in the polycrystalline samples is much lower. However, it is noteworthy that, despite a high T_c^{zero} up to ∼40 K, we failed to detect diamagnetic response in our samples. Figure S3 in Supplemental Material [37] shows the results of ac susceptibility $\chi'(T)$ of sample no. 4 measured under pressures up to 15 GPa with the mutual induction method in CAC, from which we can see only the diamagnetic signal when Pb undergoes superconducting transition. This result implies a filamentary nature for the observed superconductivity in our $La_3Ni_2O_{6.93}$ polycrystalline samples under high pressures below 15 GPa. Such a scenario can rationalize the observation that the zero-resistivity state in the pressurized $La_3Ni_2O_{6.93}$ samples is so fragile that it can be easily inhibited by increasing magnetic fields [Fig. 3(a)] and applied electrical currents (Fig. S4 [37]), or subjecting to nonhydrostatic pressure conditions [13–15]. Ongoing work is focused on understanding whether the observed superconductivity stems from undetectable impurity phases, oxygen nonstoichiometry, or unique microscopic heterostructures resulting from the intergrowth of competing phases.

IV. CONCLUSION

In summary, phase-pure polycrystalline samples of $La_3Ni_2O_{7-\delta}$ with slight oxygen deficiency were prepared via the sol-gel method without additional oxygen annealing. Such a sample exhibits a semiconductinglike electrical transport behavior with a clear upturn below $T_{DW} \approx 140$ K associated with the DW transition. Measurements of the resistivity under various hydrostatic pressures up to 18 GPa show that the DW related anomaly in resistivity is suppressed gradually by pressure and the superconductivity can emerge at pressures as low as ∼6 GPa. The superconducting transition temperature increases progressively with further increasing pressure, reaching $T_c^{onset} = 78.1$ K and $T_c^{zero} = 41$ K at 18 GPa. The constructed T-P phase diagram of $La_3Ni_2O_{6.93}$ polycrystalline samples shares similar features with that of $La_3Ni_2O_7$ crystals and reveals the close relationship between superconductivity, DW order, and the strange-metal-like behavior in this system. Although our polycrystalline $La_3Ni_2O_{6.93}$ exhibited a high $T_c^{onset} = 78.1$ K and $T_c^{zero} = 41$ K at 18 GPa, no diamagnetic effect was observed in our study, indicating a filamentary nature of the observed superconductivity at least in the studied pressure range. Further effort should be devoted to unravelling the origin of this peculiar phenomenon, with an aim to convert it to bulk superconductivity. Considering the relative ease of synthesizing uniform polycrystalline samples with controlled stoichiometry, further investigations of such samples could provide valuable insights into the underlying factors responsible for the high-temperature superconductivity observed in $La_3Ni_2O_7$.

ACKNOWLEDGMENTS

We are grateful to Professor Zhongxian Zhao for the insightful discussions and we also thank Professor Meng Wang for the previous collaboration on the $La_3Ni_2O_7$ crystals. This work is supported by the National Natural Science Foundation of China (Grants No. 12025408, No. 11921004, No. 12174424, and No. 11888101), National Key Research and Development Program of China (Grant No. 2021YFA1400200), the Strategic Priority Research Program of CAS (Grant No. XDB33000000), the China Postdoctoral Science Foundation (Grant No. 2023M743740), the Postdoctoral Fellowship Program of China Postdoctoral Science Foundation (Grant No. GZB20230828), the Specific Research Assistant Funding Program of CAS (Grant No. E3VP011X61), the CAS Project for Young Scientists in Basic Research (Grants No. 2022YSBR-047 and No. 2022YSBR-048), the Youth Innovation Promotion Association of CAS (Grant No. 2023007), and the President's International Fellowship Initiative (Grant No. 2024PG0003). J.-Q. Y was supported by the U.S. Department of Energy, Office of Science, Basic Energy Sciences, Materials Sciences and Engineering Division. The high-pressure experiments were performed at the Cubic Anvil Cell station of Synergic Extreme Condition User Facility (SECUF). This research used resources at the High Flux Isotope Reactor, a U.S. DOE Office of Science User Facility operated by the Oak Ridge National Laboratory.

[1] J. G. Bednorz and K. A. Müller, *Possible high T_c superconductivity in the* Ba − La − Cu − *O system*, Z. Phys. B **64**, 189 (1986).

[2] M. K. Wu, J. R. Ashburn, C. J. Torng, P. H. Hor, R. L. Meng, L. Gao, Z. J. Huang, Y. Q. Wang, and C. W. Chu, *Superconductivity at 93 K in a new mixed-phase Y* − Ba − Cu − *O compound system at ambient pressure*, Phys. Rev. Lett. **58**, 908 (1987).

[3] P. A. Lee, N. Nagaosa, and X. G. Wen, *Doping a Mott insulator: Physics of high-temperature superconductivity*, Rev. Mod. Phys. **78**, 17 (2006).

[4] B. Keimer, S. A. Kivelson, M. R. Norman, S. Uchida, and J. Zaanen, *From quantum matter to high-temperature superconductivity in copper oxides*, Nature (London) **518**, 179 (2015).

[5] D. Li, K. Lee, B. Y. Wang, M. Osada, S. Crossley, H. R. Lee, Y. Cui, Y. Hikita, and H. Y. Hwang, *Superconductivity in an infinite-layer nickelate*, Nature (London) **572**, 624 (2019).

[6] S. Zeng, C. S. Tang, X. Yin, C. Li, M. Li, Z. Huang, J. Hu, W. Liu, G. J. Omar, H. Jani *et al.*, *Phase diagram and superconducting dome of infinite-layer* $Nd_{1-x}Sr_xNiO_2$ *thin films*, Phys. Rev. Lett. **125**, 147003 (2020).

[7] H. Sakakibara, H. Usui, K. Suzuki, T. Kotani, H. Aoki, and K. Kuroki, *Model construction and a possibility of cupratelike pairing in a new d^9 nickelate superconductor* (Nd, Sr)NiO_2, Phys. Rev. Lett. **125**, 077003 (2020).

[8] M. Hirayama, T. Tadano, Y. Nomura, and R. Arita, *Materials design of dynamically stable d^9 layered nickelates*, Phys. Rev. B **101**, 075107 (2020).

[9] M. Osada, B. Y. Wang, K. Lee, D. Li, and H. Y. Hwang, *Phase diagram of infinite layer praseodymium nickelate* $Pr_{1-x}Sr_xNiO_2$ *thin films*, Phys. Rev. Mater. **4**, 121801(R) (2020).

[10] G. A. Pan *et al.*, *Superconductivity in a quintuple-layer square-planar nickelate*, Nat. Mater. **21**, 160 (2022).

[11] N. N. Wang *et al.*, *Pressure-induced monotonic enhancement of T_c to over 30 K in superconducting* $Pr_{0.82}Sr_{0.18}NiO_2$ *thin films*, Nat. Commun. **13**, 4367 (2022).

[12] Q. Li, C. He, J. Si, X. Zhu, Y. Zhang, and H.-H. Wen, *Absence of superconductivity in bulk* $Nd_{1-x}Sr_xNiO_2$, Commun. Mater. **1**, 16 (2020).

[13] H. Sun *et al.*, *Signatures of superconductivity near 80 K in a nickelate under high pressure*, Nature (London) **621**, 493 (2023).

[14] Y. Zhang *et al.*, *High-temperature superconductivity with zero-resistance and strange metal behaviour in* $La_3Ni_2O_7$, arXiv:2307.14819.

[15] J. Hou *et al.*, *Emergence of high-temperature superconducting phase in the pressurized* $La_3Ni_2O_7$ *crystals*, Chin. Phys. Lett. **40**, 117302 (2023).

[16] Y. Gu, C. Le, Z. Yang, X. Wu, and J. Hu, *Effective model, and pairing tendency in bilayer Ni-based superconductor* $La_3Ni_2O_7$, arXiv:2306.07275.

[17] W. Wu, Z. Luo, D.-X. Yao, and M. Wang, *Charge transfer and Zhang-Rice singlet bands in the nickelate superconductor* $La_3Ni_2O_7$ *under pressure*, arXiv:2307.05662.

[18] Y. Shen, M. Qin, and G.-M. Zhang, *Effective bi-layer model Hamiltonian and density-matrix renormalization group study for the high-T_c superconductivity in* $La_3Ni_2O_7$ *under high pressure*, Chin. Phys. Lett. **40**, 127401 (2023).

[19] X.-Z. Qu, D.-W. Qu, J. Chen, C. W. F. Yang, W. Li, and G. Su, *Bilayer t-J-$J_\perp$ model and magnetically mediated pairing in the pressurized nickelate* $La_3Ni_2O_7$, Phys. Rev. Lett. **132**, 036502 (2024).

[20] Z. Luo, X. Hu, M. Wang, W. Wú, and D.-X. Yao, *Bilayer two-orbital model of* $La_3Ni_2O_7$ *under pressure*, Phys. Rev. Lett. **131**, 126001 (2023).

[21] D.-C. Lu, M. Li, Z.-Y. Zeng, W. Hou, J. Wang, and F. Y. Y.-Z. You, *Superconductivity from doping symmetric mass generation insulators: Application to* $La_3Ni_2O_7$ *under pressure*, arXiv:2308.11195.

[22] H. Oh and Y.-H. Zhang, *Type II t-J model and shared antiferromagnetic spin coupling from Hund's rule in superconducting* $La_3Ni_2O_7$, Phys. Rev. B **108**, 174511 (2023).

[23] Y.-F. Yang, G.-M. Zhang, and F.-C. Zhang, *Minimal effective model and possible high-T_c mechanism for superconductivity of* $La_3Ni_2O_7$ *under high pressure*, Phys. Rev. B **108**, L201108 (2023).

[24] Z. Zhang, M. Greenblatt, and J. B. Goodenough, *Synthesis, structure, and properties of the layered perovskite* $La_3Ni_2O_{7-\delta}$, J. Solid State Chem. **108**, 402 (1994).

[25] S. Taniguchi, T. Nishikawa, Y. Yasui, Y. Kobayashi, J. Takeda, S.-i. Shamoto, and M. Sato, *Transport, magnetic and thermal properties of* $La_3Ni_2O_{7-\delta}$, J. Phys. Soc. Jpn. **64**, 1644 (1995).

[26] C. D. Ling, D. N. Argyriou, G. Wu, and J. J. Neumeier, *Neutron diffraction study of* $La_3Ni_2O_7$*: Structural relationships among* $n = 1$*, 2, and 3 phases* $La_{n+1}Ni_nO_{3n+1}$, J. Solid State Chem. **152**, 517 (2000).

[27] G. Wu, J. J. Neumeier, and M. F. Hundley, *Magnetic susceptibility, heat capacity, and pressure dependence of the electrical resistivity of* $La_3Ni_2O_7$ *and* $La_4Ni_3O_{10}$, Phys. Rev. B **63**, 245120 (2001).

[28] G. Amow, I. Davidson, and S. Skinner, *A comparative study of the Ruddlesden-Popper series,* $La_{n+1}Ni_nO_{3n+1}$ *(*$n = 1$*, 2 and 3), for solid-oxide fuel-cell cathode applications*, Solid State Ionics **177**, 1205 (2006).

[29] V. V. Poltavets, K. A. Lokshin, T. Egami, and M. Greenblatt, *The oxygen deficient Ruddlesden–Popper* $La_3Ni_2O_{7-\delta}$ *(*$\delta = 0.65$*) phase: Structure and properties*, Mater. Res. Bull. **41**, 955 (2006).

[30] J. Zhang, H. Zheng, Y.-S. Chen, Y. Ren, M. Yonemura, A. Huq, and J. F. Mitchell, *High oxygen pressure floating zone growth and crystal structure of the metallic nickelates* $R_4Ni_3O_{10}$ *(*$R =$ La, Pr*)*, Phys. Rev. Mater. **4**, 083402 (2020).

[31] Z. Zhang and M. Greenblatt, *Synthesis, structure, and properties of* $Ln_4Ni_3O_{10-\delta}$ *(*$Ln =$ La, Pr*, and* Nd*)*, J. Solid State Chem. **117**, 236 (1995).

[32] V. O. Garlea, B. C. Chakoumakos, S. A. Moore, G. B. Taylor, T. Chae, R. G. Maples, R. A. Riedel, G. W. Lynn, and D. L. Selby, *The high-resolution powder diffractometer at the high flux isotope reactor*, Appl. Phys. A **99**, 531 (2010).

[33] S. Calder *et al.*, *A suite-level review of the neutron powder diffraction instruments at Oak Ridge National Laboratory*, Rev. Sci. Instrum. **89**, 092701 (2018).

[34] J. G. Cheng, B. S. Wang, J. P. Sun, and Y. Uwatoko, *Cubic anvil cell apparatus for high-pressure and low-temperature physical property measurements*, Chin. Phys. B **27**, 077403 (2018).

[35] K. Ishigaki, J. Gouchi, S. Nagasaki, J. G. Cheng, and Y. Uwatoko, *Development of two-stage multi-anvil apparatus for low-temperature measurements*, Pap. Phys. **11**, 110006 (2019).

[36] V. I. Voronin, I. F. Berger, V. A. Cherepanov, L. Y. Gavrilova, A. N. Petrov, A. I. Ancharov, B. P. Tolochko, and S. G. Nikitenko, *Neutron diffraction, synchrotron radiation and EXAFS spectroscopy study of crystal structure peculiarities of the lanthanum nickelates* $La_{n+1}Ni_nO_y$ *(*$n = 1, 2, 3$*)*, Nucl. Instrum. Methods Phys. Res., Sect. A **470**, 202 (2001).

[37] See Supplemental Material at http://link.aps.org/supplemental/10.1103/PhysRevX.14.011040 for the results of the NPD refinements with different space groups of *Amam* vs *Fmmm*, ac magnetic susceptibility under various pressures up to 15 GPa, and the resistivity data at 18 GPa measured with different currents.